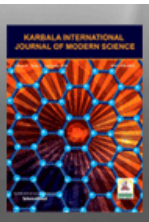

Karbala International Journal of Modern Science

Volume 6 | Issue 2 Article 13

Transition state theory application to H2 gas sensitivity of pristine and Pd doped SnO2 clusters

Mudar Ahmed Abdulsattar
Ministry of Science and Technology, Baghdad, Iraq, mudarahmed3@yahoo.com

Transition state theory application to H2 gas sensitivity of pristine and Pd doped SnO2 clusters

Abstract

The reaction of H_2 and O_2 gases with pristine and Pd doped $Sn_{10}O_{16}$ clusters is investigated using transition state theory and density functional theory. The reaction of hydrogen and oxygen molecules is controlled by a transition state that implies crossing an activation energy hill to react with the SnO_2 cluster. Our investigation performs thermodynamic calculations, including Gibbs free energy, enthalpy, and entropy of activation and reaction in the temperature range 25-500 °C. The results show that the Gibbs free energy of activation of H_2 gas reaction is 0.23 and 0.18 eV for pristine and Pd doped $Sn_{10}O_{16}$ respectively at standard conditions. The reduction of 0.05 eV of the activation barrier is enough to raise the reaction rate constant by a factor of 7 between pristine and Pd doped at standard conditions. The temperature-dependent reaction rate increases continuously as the temperature increases in the investigated range. A double exponential function describes the time dependence of cluster concentration. Variation of energy gaps due to the H_2 reaction explains the sensitivity values of present clusters to H_2 molecules.

Keywords

SnO2; H2: Pd; Gas sensor; Transition state.

1. Introduction

Tin dioxide is the most used material in gas sensing [1−5]. SnO_2 alone has a relatively lower sensitivity to environmentally polluting and other gases. To raise sensitivity, several kinds of surface catalysts, such as Pd and Pt, are used [6−10]. The use of nanoparticles usually enhances the sensing operation due to the higher surface area of particles [11,12]. Many other factors affect sensing effectiveness of SnO_2 such as temperature, the method used to manufacture SnO_2 films, the kind of reaction, …etc.

Theoretical aspects of the sensing mechanisms are less investigated than experimental procedures [13−15]. Most of these calculations use density functional theory to calculate adsorption mechanisms [16]. Transition state theory, which is the most promising theory in reaction kinetics, has been rarely applied to gas sensors [17]. This theory investigates the existence of a transition state with positive Gibbs free energy of activation of incident gas particles near the surface of the gas sensor. The transition state theory had been applied extensively to explain many reaction mechanisms [18−20]. In the present work, we apply transition state theory to calculate the transition rate and sensitivity of SnO_2 clusters to H_2 gas as a function of temperature. In addition to the application to the sensitivity of SnO_2 clusters to H_2 gas, the effect of palladium surface doping is also investigated. Pd is one of the well-known catalysts that reduce the value of Gibbs free energy of activation to promote higher reaction rates and better sensitivity [21−23]. Pd was widely used experimentally in SnO_2 gas sensors with limited published theoretical transition state theory explanations [24−27]. The novelty of the present work lies in the fact that many experimental gas sensing results of sometimes contradicting directions are not explained. A theory that can collect and explain the experimental results, in our opinion, can be anticipated from the transition state theory used in the present work.

2. Theory

SnO_2 clusters are repeatedly suggested to represent surfaces of gas sensors to illustrate the sensing mechanism [13,28−30]. In the present work, we use pyramidal cluster $Sn_{10}O_{16}$ for the representation of the SnO_2 cluster [31,32]. Surface pyramids are well-known on SnO_2 surfaces [33−35], so it is logical to use these pyramids to represent the interacting surface of a sensor. The size of these clusters is suitable to include the interaction of several atomic neighbors with the interacting gas molecule. SnO_2 is known with oxygen-deficiency property [36,37]. To probe what stoichiometry does this cluster prefers, we simulated the thermodynamics of the following reactions at standard temperature and pressure:

$$Sn_{10}O_{14} + O_2 \rightarrow Sn_{10}O_{16} (\Delta G_r = -0.1732 \text{ eV}). \quad (1)$$

$$Sn_{10}O_{16} + O_2 \rightarrow Sn_{10}O_{18} (\Delta G_r = 0.01073 \text{ eV}). \quad (2)$$

$$Sn_{10}O_{18} + O_2 \rightarrow Sn_{10}O_{20} (\Delta G_r = 0.02515 \text{ eV}). \quad (3)$$

In the above equations, ΔG_r is the change in Gibbs free energy of the reaction. All the above and forthcoming values are calculated using B3LYP hybrid functional in density functional theory with SDD basis for heavy atoms (Sn and Pd) and 6-311G** basis for the lighter ones [38]. Gaussian 9 program is used to perform the calculations [39]. In Eq. (1) we can see that the cluster $Sn_{10}O_{14}$ is unstable and converts to $Sn_{10}O_{16}$ when it is exposed to oxygen in the air as indicated by the negative value of the Gibbs free energy. On the other hand, $Sn_{10}O_{16}$ is more stable than $Sn_{10}O_{18}$ and $Sn_{10}O_{20}$ from the values of Gibbs free energy of the reactions in Eqs. (2) and (3). The oxygen-deficiency is evident from the existence of lower oxygen stoichiometry (SnO) of Sn [40]. The higher oxygen content oxide (SnO_2) tries to loss oxygen to be closer to the lower oxygen content oxide (SnO) by creating oxygen vacancies. Fig. (1a) shows the cluster $Sn_{10}O_{16}$, while Fig. (1b) shows the cluster Sn_9PdO_{16} in which one Sn atom is replaced by a palladium atom to simulate the doping effect on gas sensing operation. Figs. (1c) and (1d) shows the oxygen-reduced clusters $Sn_{10}O_{15}$ and Sn_9PdO_{15} of pristine and Pd doped clusters, respectively. When H_2 molecules pass over $Sn_{10}O_{16}$ molecule, one H_2 molecule will pick one oxygen atom according to the reaction:

$$Sn_{10}O_{16} + H_2 \rightarrow Sn_{10}O_{15} + H_2O (\Delta G_r = -1.508 \text{ eV}). \quad (4)$$

Although this reaction has negative Gibbs free energy of reaction, the reaction rate is controlled by a transition state with positive Gibbs free energy of reaction as follows at standard temperature and pressure:

https://doi.org/10.33640/2405-609X.1615

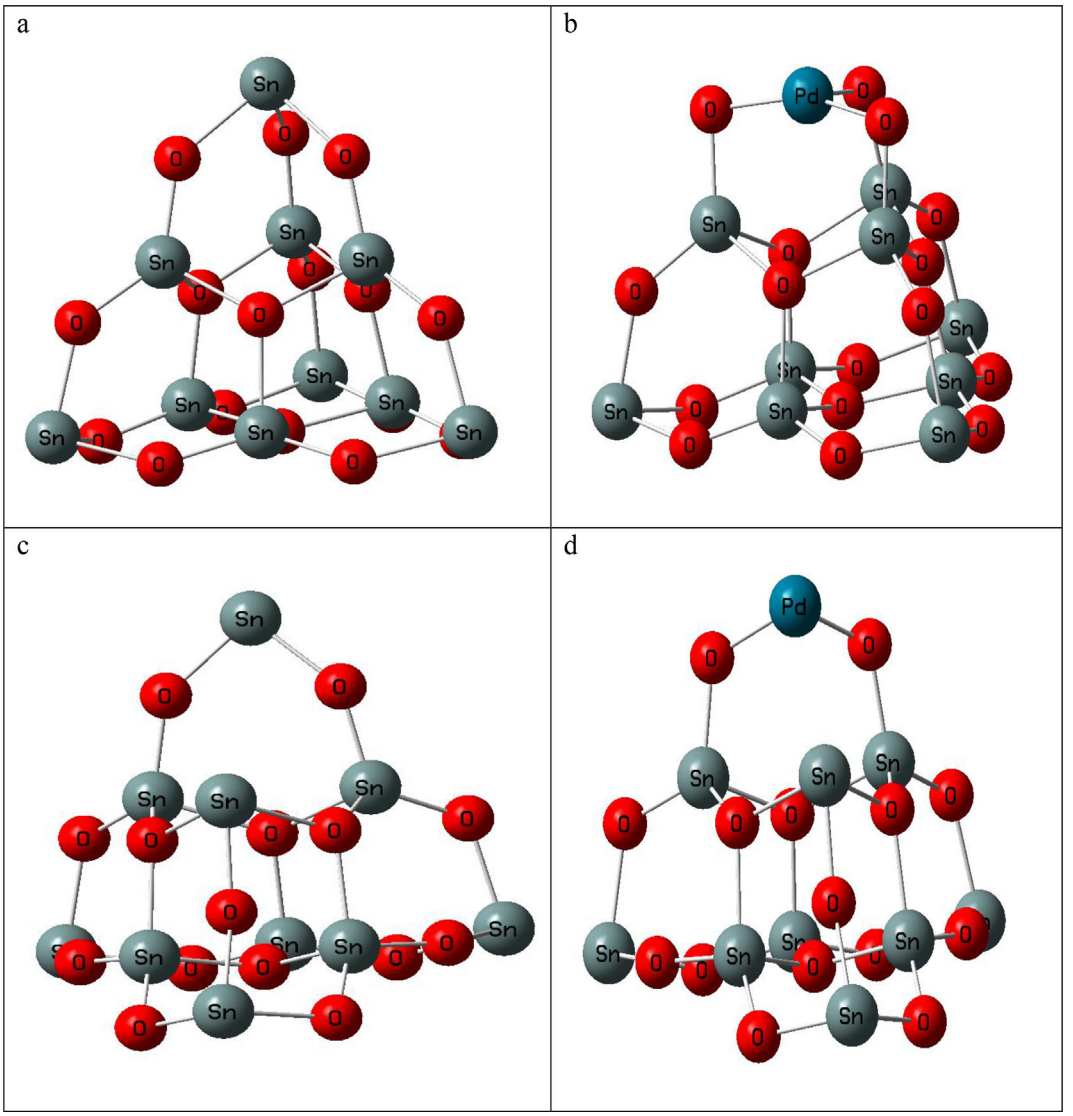

Fig. 1. (a) shows the cluster $Sn_{10}O_{16}$ while (b) shows the cluster Sn_9PdO_{16} in which one Sn atom is replaced by a palladium atom to simulate the doping effect on gas sensing operation. (c) and (d) shows the oxygen-reduced clusters $Sn_{10}O_{15}$ and Sn_9PdO_{15} of pristine and Pd doped clusters, respectively.

$$Sn_{10}O_{16} + H_2 \rightarrow Sn_{10}O_{16}\ldots H_2 (\Delta G_r = 0.231\ eV). \quad (5)$$

The attachment of the H_2 molecule at the $Sn_{10}O_{16}$ surface in the above equation ($Sn_{10}O_{16}\ldots H_2$) by the van der Waals forces is represented by the three points (…) between $Sn_{10}O_{16}$ and H_2 in Eq. (5) above. This transition state represents a barrier that must be overcome by hydrogen molecules to be able to interact with the $Sn_{10}O_{16}$ cluster. The same is true for the Pd doped clusters. These H_2 transition states are shown in Fig. (2) for the pristine ($Sn_{10}O_{16}$) and Pd doped clusters (Sn_9PdO_{15}).

The H_2 and O_2 molecules are added at 3 Å distance at the beginning as recommended by transition state evaluation procedure of Gaussian 09 program. The optimization procedure moves the molecules to the most energy attractive position. This position was 4.048 and 4.237 Å distance for H_2 and O_2 molecules respectively from the nearest atom in SnO_2 cluster in the pristine case. For the Pd doped cluster, the distances are 3.94 and 3.05 Å respectively. H_2 molecules prefers to approach O atoms that are near Sn corner atoms while O_2 molecules approaches towards Sn corner atoms.

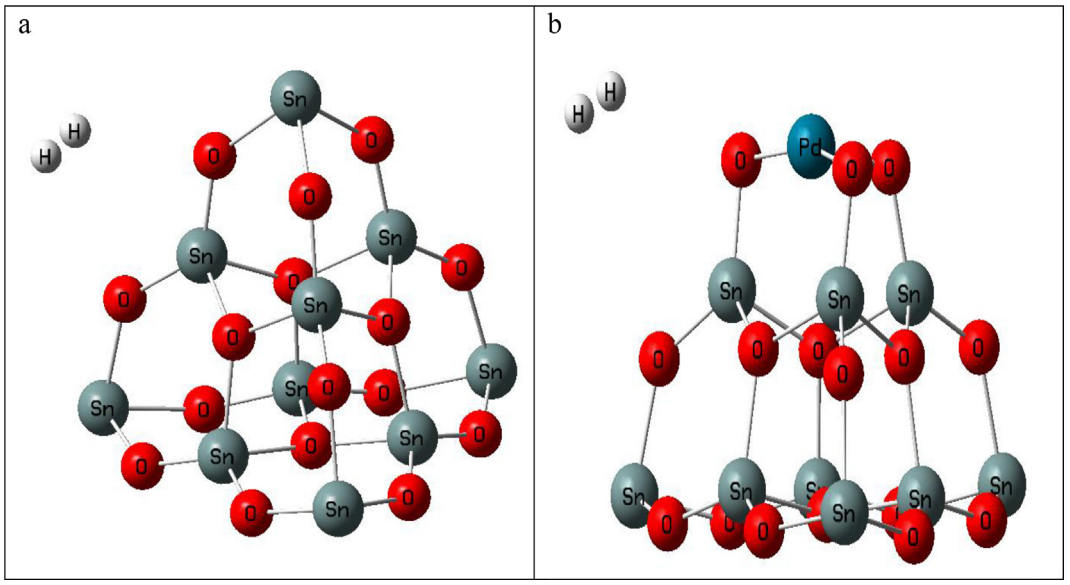

Fig. 2. This figure shows the H_2 molecule transition state in (a) pristine $Sn_{10}O_{16}$ cluster, and (b) Pd doped Sn_9PdO_{16} cluster.

3. Results and discussion

Fig. (3) shows the variation of the Gibbs free energy of the three cases of H_2 interaction states with $Sn_{10}O_{16}$ and Sn_9PdO_{16} clusters. Taking the reference zero Gibbs energy point of H_2 molecule to be very far from $Sn_{10}O_{16}$ or Sn_9PdO_{16} clusters, the activation and reaction energies are shown. As we can see from Fig. (3) that the values of the activation energies are small compared to the reaction energies. As a result of small values of activation energies, all the incident particles reaching the hilltop at the transition state will

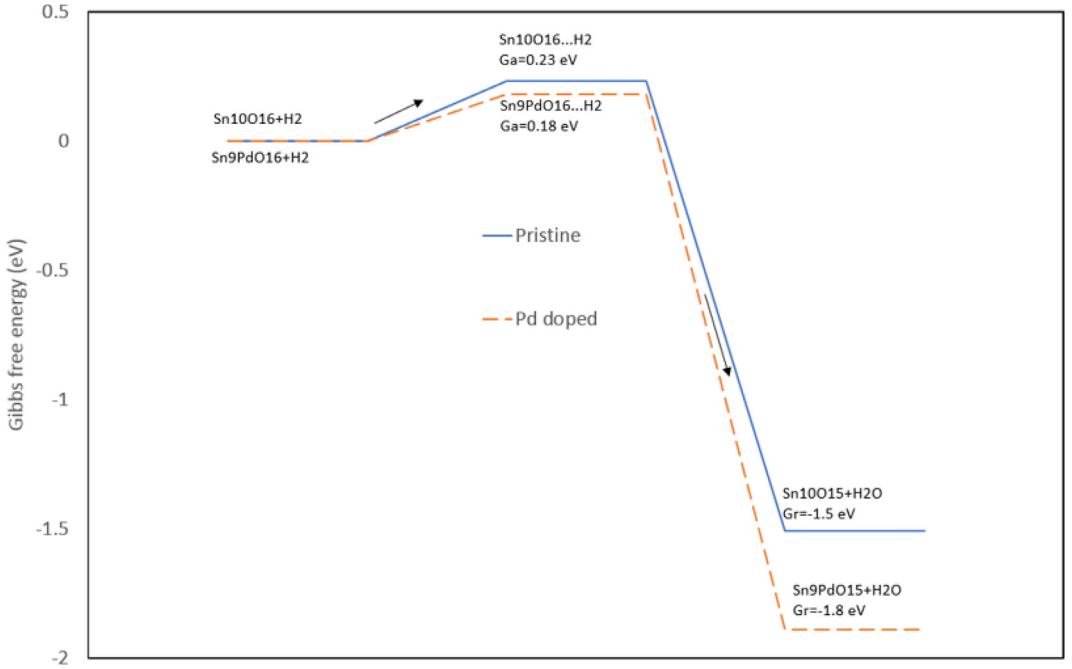

Fig. 3. Gibbs free energy of activation and reaction of $Sn_{10}O_{16}$ and Sn_9PdO_{16} with H_2.

eventually react with the target clusters with a negligible number of H_2 molecules that turn back to the outer space.

The rate at which the number of $Sn_{10}O_{16}$ clusters react with H_2 molecules is given by Ref. [39]:

$$\frac{d[Sn_{10}O_{16}]}{dt} = -C[Sn_{10}O_{16}][H_2]k(T). \quad (6)$$

In the above equation $[Sn_{10}O_{16}]$ and $[H_2]$ are the concentration of $Sn_{10}O_{16}$ and H_2, respectively, and T is the temperature. The minus sign indicates the decrease in the number of $Sn_{10}O_{16}$ clusters as a result of the interaction with H_2 molecules. k(T) is called the reaction rate constant that is given by:

$$k(T) = Te^{\left(\frac{-\Delta G_a}{k_B T}\right)} \quad (7)$$

In the above equation, ΔG_a is the activation energy, and k_B is Boltzmann constant. C is a constant that must be determined experimentally. We shall call this parameter the materials constant. From Eq. (6), we can get the following equation:

$$[Sn_{10}O_{16}] = [Sn_{10}O_{16}]_0 e^{-C[H_2]k(T)t} \quad (8)$$

In the above equation, $[Sn_{10}O_{16}]_0$ is the concentration at the beginning of the exposure to $[H_2]$ molecules. In the gas sensing literature, the response and recovery times are defined to be 90% of the saturation values reached, i.e., only 10% of the saturation values remained. Using this definition, we can define the meantime (τ) and decay constant (λ) by:

$$\frac{[Sn_{10}O_{16}]}{[Sn_{10}O_{16}]_0} = 0.1 = e^{-\frac{t_{response}}{\tau}} = e^{-\lambda t_{response}} \quad (9)$$

$$\lambda = \frac{ln(0.1)}{-t_{response}} = \frac{1}{\tau} \quad (10)$$

From Eqs. (7) and (8) we have:

$$\lambda = C[H_2]k(T) = C[H_2]Te^{\left(\frac{-\Delta G_a}{k_B T}\right)}. \quad (11)$$

The double exponential function can give the final concentration equation:

$$[Sn_{10}O_{16}] = [Sn_{10}O_{16}]_0 e^{-C[H_2]Te^{\left(\frac{-\Delta G_a}{k_B T}\right)}t} \quad (12)$$

Although ΔG_a in the above equation can be determined from transition state theory calculations, there is no way that the C constant can be determined theoretically. This constant reflects the structure, geometry, particle size, the ability of the incident gas to diffuse in the target material, and many other factors inhibited in the method used to manufacture the gas sensor. It effectively illustrates the surface area that is available for reacting.

In the case of the recovery period ($Sn_{10}O_{15} + ½O_2 \rightarrow Sn_{10}O_{16}$), oxygen reacts with the formed $Sn_{10}O_{15}$ clusters to transform them back to $Sn_{10}O_{16}$ clusters. Eq. (12) for the case of recovery period reads:

$$[Sn_{10}O_{15}] = [Sn_{10}O_{15}]_0 e^{-C[O2]Te^{\left(\frac{-\Delta G_a}{k_B T}\right)}t} \quad (13)$$

Since oxygen concentration $[O_2]$ is nearly constant in air and will not be changed by the minimal amounts of oxygen absorbed in the reaction, $[O_2]$ term can be absorbed by the C constant in Eq. (13). The values of the C constant for H_2 and O_2 are 0.4 and 0.00524 $(ppm.K.sec)^{-1}$ respectively for the pristine SnO_2 molecule.

The energy gap of materials is related to the electrical conductivity by the following equations [41]:

$$\sigma = \sigma_0 \exp\left(\frac{-E_g}{2k_B T}\right) \quad (14)$$

The energy gaps of $Sn_{10}O_{15}$ and $Sn_{10}O_{16}$ from our calculations are 3.537 and 3.841 eV, respectively. Assuming σ_0 is the same for the two molecules and using the above equation, the response (R) which is defined as the ratio of the resistivity (reciprocal of conductivity) of $Sn_{10}O_{15}$ to that of $Sn_{10}O_{16}$ is given by the Equation:

$$R = \frac{R_a}{R_g} = \exp\left(E_{ga} - E_{gg}\right) \quad (15)$$

In the above equation, R_a and E_{ga} are the resistance and energy gap when only atmospheric air is above the sensor. R_g and E_{gg} are for the existence of H_2 gas over the sensor. According to previously mentioned values of gaps, the value of (R) is 1.355. This value is the lowest possible ratio and can be increased by continuous exposure to H_2 or other gases [42]. As a result of continued exposure to H_2, islands of pure Sn_{10} clusters are created, and all the oxygen in $Sn_{10}O_{16}$ is reduced. The energy gap of the Sn_{10} cluster is 1.615 eV. The value of the calculated response, in this case, is 9.26. The present results are in good agreement with that of reference [43] in which the response for low H_2 concentration (equal or less than 250 ppm) is in the range (1–2) and reaches 6.5 for 1000 ppm concentration.

Higher temperatures and concentrations can make small islands of Sn metal coalesce, forming bigger clusters that have smaller energy gaps and smaller resistivity, as proved by quantum confinement theory [44].

Fig. (4) shows the variation of Gibbs free energy of activation as a function of temperature for both pristine and Pd doped cases, including response and recovery with O_2 and H_2 gases, respectively. We can see that in the H_2 case, this energy increases with temperature and that pristine activation energy is always higher than Pd doped case. The activation Gibbs energies for the O_2 recovery are higher than that of H_2 response, meaning lower reaction rates for the same incident number of H_2 and O_2 molecules. However, this is not the case practically since the incident H_2 molecules are much less than O_2 molecules (O_2 molecules comprise 20.9% of atmospheric air). These results are obtained from ab initio DFT calculations with no fitting of empirical parameters.

Fig. (5) shows the values of the reaction rate constant k(T) as a function of temperature. We can see that although the values of Gibbs free energy increase in Fig. (4), the reaction rate constant also increases because of the effect of the temperature variable at the beginning and exponential term in Eq. (7). The very high values of the O_2 Gibbs free energy of reaction activation results in a meager reaction rate constant. These results are obtained from ab initio DFT calculations with no fitting or empirical parameters.

In gas sensor experiments the sensor is first exposed to the detected gas (in the present case H_2) that take some oxygen from the material. Then the detected gas is stopped and usual air (that contains 20.9% oxygen) is passed over the sensitive material and the material regains its lost oxygen. Fig. (6) shows the variation of the concentration of $Sn_{10}O_{16}$ and $Sn_{10}O_{15}$ molecules with time using Eqs. (9)–(13) for H_2 and O_2. The value of the materials constant is calculated from Ref. [43] results. Reference [43] assigns 15 and 4 s for the response and recovery times, respectively. Since the resistivity of the $Sn_{10}O_{15}$ cluster is lower than that of $Sn_{10}O_{16}$, the variation of concentration $[Sn_{10}O_{15}]$ can also approximately represent the variation of resistance when an H_2 gas passes over the sensing material using a suitable constant.

Gibbs free energy of activation consists of two parts:

$$\Delta G_a = \Delta H_a - \Delta S_a T \tag{16}$$

In Eq. (16) ΔH_a and ΔS_a are the enthalpy and entropy of activation, respectively. Table 1 shows the values of the calculated thermodynamic quantities of activation and reaction of doped and pristine clusters at standard temperature and pressure. We can see from Table (1) that all Gibbs free energies of activation are

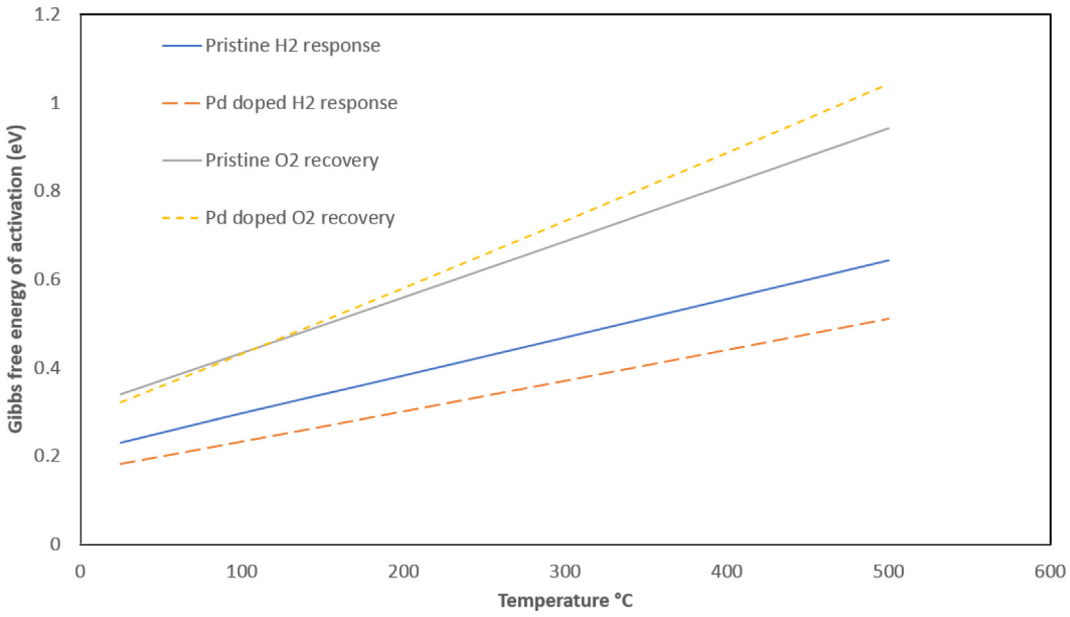

Fig. 4. Gibbs free energy of activation as a function of the temperature of pristine and Pd doped clusters response and recovery with H_2 and O_2 gases, respectively.

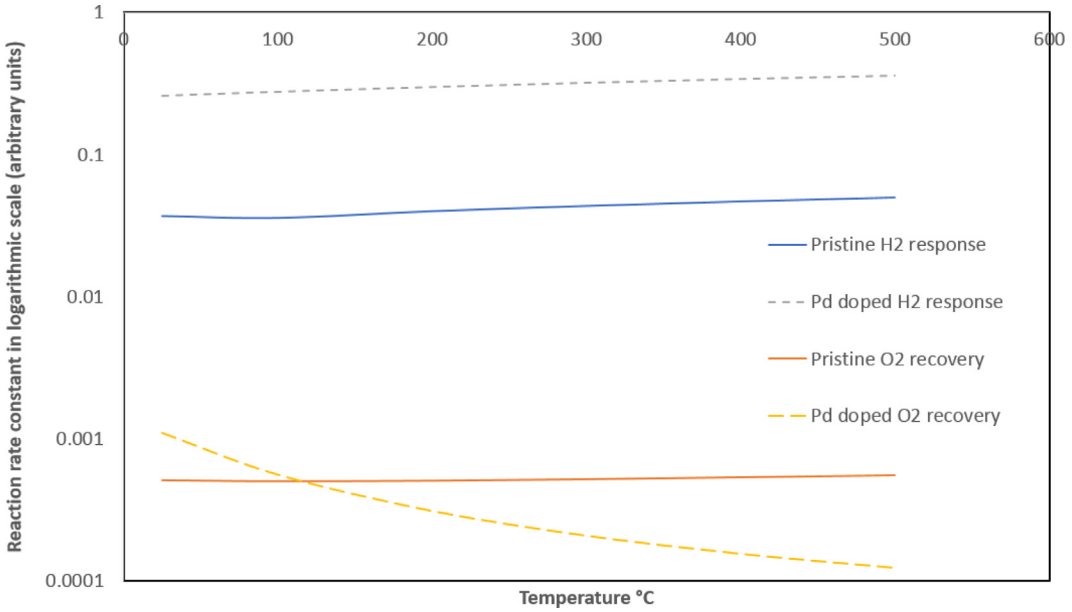

Fig. 5. The reaction rate constant as a function of the temperature of pristine and Pd doped clusters response and recovery with H_2 and O_2 gases, respectively. The logarithmic scale is used for the y-axis.

positive, while all Gibbs free energies of reaction are negative. However, all enthalpies are negative, which means that all activations and reactions are exothermic. All entropies are negative, except reactions 5 and 6 in Table (1). Entropies are positive when the number of product molecules is less than interacting molecules as in reactions 5 and 6. From Eq. (16) positive entropies enhances the reaction probability by making Gibbs free energies more negative as in reactions 5 and 6 in Table (1). Finally, we added the heat capacity at constant volume in Table (1) that indicates the change in temperature due to the proceeding reaction. Positive

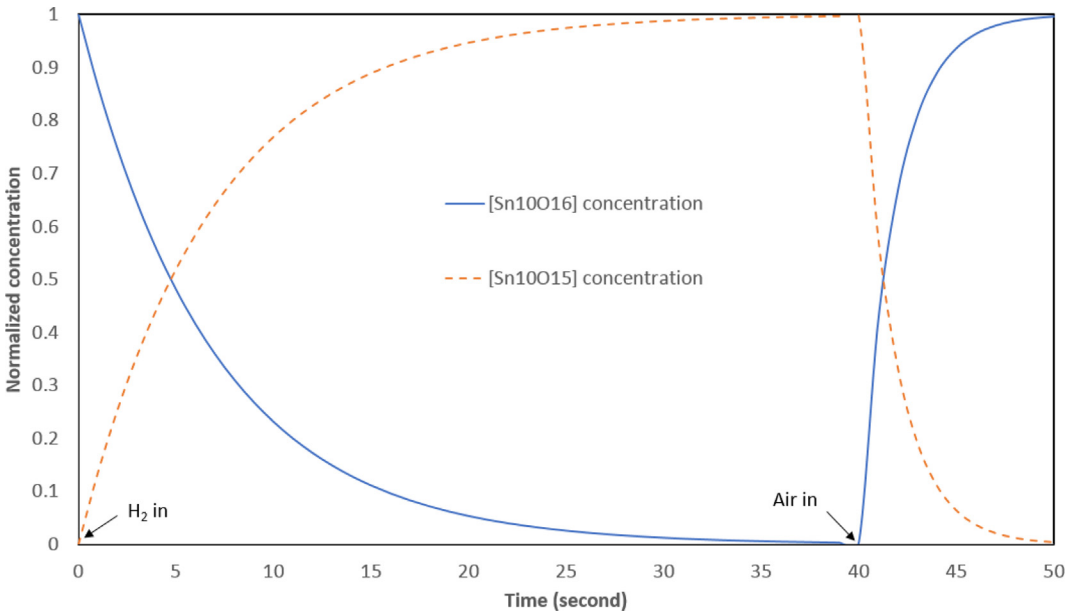

Fig. 6. Variation of normalized concentrations of $Sn_{10}O_{16}$ and $Sn_{10}O_{15}$ clusters as a function of time due to interaction with H_2 (until 40 s) and O_2 molecules in the air (40–50 s) at 300 °C normalized to Refs. [43] values.

Table 1
The thermodynamic quantities of interacting of pristine and Pd doped $Sn_{10}O_{16}$ clusters with H_2 and O_2 gases are shown in this table at standard temperature and pressure (temperature 298.15 K and pressure 1 atm).

n	Activation reactions	ΔG_a (eV)	ΔH_a (eV)	ΔS_a (cal/mol-K)	ΔC_{va} (cal/mol-K)
1	$Sn_{10}O_{16} + H_2 \rightarrow Sn_{10}O_{16}...H_2$	0.231	−0.0192	−19.372	0.808
2	$Sn_9PdO_{16} + H_2 \rightarrow Sn_9PdO_{16}...H_2$	0.181	−0.0185	−15.448	0.951
3	$Sn_{10}O_{15} + O_2 \rightarrow Sn_{10}O_{15}...O_2$	0.341	−0.0295	−28.644	0.984
4	$Sn_9PdO_{15} + O_2 \rightarrow Sn_9PdO_{15}...O_2$	0.321	−0.1098	−33.365	−0.906
	Final reactions	ΔG_r (eV)	ΔH_r (eV)	ΔS_r (cal/mol-K)	ΔC_{vr} (cal/mol-K)
5	$Sn_{10}O_{16} + H_2 \rightarrow Sn_{10}O_{15}+H_2O$	−1.508	−1.355	11.858	−3.521
6	$Sn_9PdO_{16} + H_2 \rightarrow Sn_9PdO_{15}+H_2O$	−1.891	−1.721	13.16	−3.502
7	$Sn_{10}O_{15} + ½O_2 \rightarrow Sn_{10}O_{16}$	−1.318	−1.594	−21.303	2.052
8	$Sn_9PdO_{15} + ½O_2 \rightarrow Sn_9PdO_{16}$	−0.936	−1.228	−22.605	2.033

change in heat capacity is usually accompanied by the reduction of temperature of sensing material and vice versa.

4. Conclusions

The thermodynamic quantities of the interaction of SnO_2 clusters with H_2 gas and O_2 are evaluated using transition state theory and density functional theory. The transition state theory implies activation of Gibbs free energy to overcome for the reaction to take place. The results show that the Pd doped cluster has lower activation energy than the pristine SnO_2 cluster. The O_2 activation energies are higher than that of H_2, resulting in a very lower reaction rate for equal amounts of incident H_2 and O_2 molecules. However, this is compensated by the higher concentration of O_2 molecules in the ambient atmosphere. The energy gap of the reactant and product molecules can be used to estimate the value of the response of a sensor. We can learn the degree of oxygen reduction from response values and H_2 concentration. The components of the Gibbs free energy of activation, i.e., entropy and enthalpy of activation can be used to explain the variation of the values of Gibbs free energy. All enthalpies of activation and reaction are negative, meaning that all the activations and reactions are exothermic. All entropies are negative except H_2 reactions. The negative entropy enhances H_2 reactions due to the conservation of the number of molecules between reactants and products.

References

[1] W. Zeng, Y. Liu, J. Mei, C. Tang, K. Luo, S. Li, H. Zhan, Z. He, Hierarchical SnO2−Sn3O4 heterostructural gas sensor with high sensitivity and selectivity to NO2, Sensor. Actuator. B Chem. 301 (2019), https://doi.org/10.1016/j.snb.2019.127010.

[2] X. Meng, Q. Zhang, S. Zhang, Z. He, The enhanced H2 selectivity of SnO2 gas sensors with the deposited SiO2 filters on surface of the sensors, Sensors (2019) 19, https://doi.org/10.3390/s19112478.

[3] L. Jin, W. Chen, S. Tang, Z. Song, Metal-doped SnO2 based H2/C2H2 gas sensor array and its detection characteristics, Yi Qi Yi Biao Xue Bao/Chinese, J. Sci. Instrum. 40 (2019) 144−152, https://doi.org/10.19650/j.cnki.cjsi.J1904760.

[4] P.G. Choi, N. Izu, N. Shirahata, Y. Masuda, Fabrication and H2-sensing properties of SnO2 nanosheet gas sensors, ACS Omega 3 (2018) 14592−14596, https://doi.org/10.1021/acsomega.8b01635.

[5] D.E. Motaung, G.H. Mhlongo, P.R. Makgwane, B.P. Dhonge, F.R. Cummings, H.C. Swart, S.S. Ray, Ultra-high sensitive and selective H2 gas sensor manifested by interface of n−n heterostructure of CeO2-SnO2 nanoparticles, Sensor. Actuator. B Chem. 254 (2018) 984−995, https://doi.org/10.1016/j.snb.2017.07.093.

[6] J. Zhang, L. Zhang, D. Leng, F. Ma, Z. Zhang, Y. Zhang, W. Wang, Q. Liang, J. Gao, H. Lu, Nanoscale Pd catalysts decorated WO3−SnO2 heterojunction nanotubes for highly sensitive and selective acetone sensing, Sensor. Actuator. B Chem. 306 (2020), https://doi.org/10.1016/j.snb.2019.127575.

[7] K. Hu, F. Wang, H. Liu, Y. Li, W. Zeng, Enhanced hydrogen gas sensing properties of Pd-doped SnO2 nanofibres by Ar plasma treatment, Ceram. Int. 46 (2020) 1609−1614, https://doi.org/10.1016/j.ceramint.2019.09.132.

[8] L. Shokrzadeh, P. Mohammadi, M.R. Mahmoudian, W.J. Basirun, M. Bahreini, L-glycine-assisted synthesis of SnO2/Pd nanoparticles and their application in detection of biodeteriorating fungi, Mater. Chem. Phys. 240 (2020), https://doi.org/10.1016/j.matchemphys.2019.122172.

[9] S. Navazani, M. Hassanisadi, M.M. Eskandari, Z. Talaei, Design and evaluation of SnO2-Pt/MWCNTs hybrid system as room temperature-methane sensors, Synth. Met. 260 (2020), https://doi.org/10.1016/j.synthmet.2019.116267.

[10] H. Cai, H. Liu, T. Ni, Y. Pan, Y. Zhao, Y. Zhu, Controlled synthesis of Pt doped SnO2 mesoporous hollow nanospheres for highly selective and rapidly detection of 3-hydroxy-2-butanone biomarker, Front. Chem. 7 (2019), https://doi.org/10.3389/fchem.2019.00843.

[11] Z. Zhang, Z. Gao, R. Fang, H. Li, W. He, C. Du, UV-assisted room temperature NO2 sensor using monolayer graphene decorated with SnO2 nanoparticles, Ceram. Int. 46 (2020) 2255−2260, https://doi.org/10.1016/j.ceramint.2019.09.211.

[12] N.S.A. Eom, H.-B. Cho, H.-R. Lim, B.S. Kim, Y.-H. Choa, Facile tilted sputtering process (TSP) for enhanced H2S gas response over selectively loading Pt nanoparticles on SnO2 thin films, Sensor. Actuator. B Chem. 300 (2019) 127009, https://doi.org/10.1016/j.snb.2019.127009.

[13] N. Zhang, Y. Fan, Y. Lu, C. Li, J. Zhou, X. Li, S. Adimi, S. Ruan, Synthesis of au-decorated SnO2 crystallites with exposed (221) facets and their enhanced acetylene sensing properties, Sensor. Actuator. B Chem. 307 (2020), https://doi.org/10.1016/j.snb.2019.127629.

[14] W. Li, C. Ding, J. Li, Q. Ren, G. Bai, J. Xu, Sensing mechanism of Sb, S doped SnO2 (1 1 0) surface for CO, Appl. Surf. Sci. 502 (2020), https://doi.org/10.1016/j.apsusc.2019.144140.

[15] Y. Zhen, J. Zhang, W. Wang, Y. Li, X. Gao, H. Xue, X. Liu, Z. Jia, Q. Xue, J. Zhang, Y. Yan, N.S. Alharbi, T. Hayat, Embedded SnO2/Diatomaceous earth composites for fast humidity sensing and controlling properties, Sensor. Actuator. B Chem. 303 (2020), https://doi.org/10.1016/j.snb.2019.127137.

[16] Q. Wang, J. Hao, H. Huang, H. Huang, M. Zhou, Q. Zhou, Adsorption energy and charge transfer of tin oxide to characteristic gases dissolved in transformer oil, in: ICHVE 2016 - 2016 IEEE Int. Conf. High Volt. Eng. Appl., Institute of Electrical and Electronics Engineers Inc., 2016, https://doi.org/10.1109/ICHVE.2016.7800905.

[17] Y. Mo, H. Li, K. Zhou, X. Ma, Y. Guo, S. Wang, L. Li, Acetone adsorption to (BeO) 12 , (MgO) 12 and (ZnO) 12 nanoparticles and their graphene composites: a density functional theory (DFT) study, Appl. Surf. Sci. 469 (2019) 962–973, https://doi.org/10.1016/j.apsusc.2018.11.079.

[18] E.F.V. de Carvalho, G.D. Vicentini, T.V. Alves, O. Roberto-Neto, Variational transition state theory rate constants and H/D kinetic isotope effects for CH3 + CH3OCOH reactions, J. Comput. Chem. (2019), https://doi.org/10.1002/jcc.26092.

[19] M.V.C.S. Rezende, N.D. Coutinho, F. Palazzetti, A. Lombardi, V.H. Carvalho-Silva, Nucleophilic substitution vs elimination reaction of bisulfide ions with substituted methanes: exploration of chiral selectivity by stereodirectional first-principles dynamics and transition state theory, J. Mol. Model. 25 (2019), https://doi.org/10.1007/s00894-019-4126-0.

[20] L.P. Viegas, Multiconformer transition state theory rate constants for the reaction between OH and α,ω-dimethoxy-fluoropolyethers, Int. J. Chem. Kinet. 51 (2019) 358–366, https://doi.org/10.1002/kin.21259.

[21] M.S. Barbosa, P.H. Suman, J.J. Kim, H.L. Tuller, J.A. Varela, M.O. Orlandi, Gas sensor properties of Ag- and Pd-decorated SnO micro-disks to NO2, H2 and CO: catalyst enhanced sensor response and selectivity, Sensor. Actuator. B Chem. 239 (2017) 253–261, https://doi.org/10.1016/j.snb.2016.07.157.

[22] Oblov Samotaev, Etrekova Litvinov, SnO2-Pd as a gate material for the capacitor type gas sensor, Proceedings 14 (2019) 10, https://doi.org/10.3390/proceedings2019014010.

[23] D. Nagai, M. Nishibori, T. Itoh, T. Kawabe, K. Sato, W. Shin, Ppm level methane detection using micro-thermoelectric gas sensors with Pd/Al2O3 combustion catalyst films, Sensor. Actuator. B Chem. 206 (2015) 488–494, https://doi.org/10.1016/j.snb.2014.09.059.

[24] L. Xiao, S. Xu, G. Yu, S. Liu, Efficient hierarchical mixed Pd/SnO2 porous architecture deposited microheater for low power ethanol gas sensor, Sensor. Actuator. B Chem. 255 (2018) 2002–2010, https://doi.org/10.1016/j.snb.2017.08.216.

[25] L. Yang, Z. Wang, X. Zhou, X. Wu, N. Han, Y. Chen, Synthesis of Pd-loaded mesoporous SnO2 hollow spheres for highly sensitive and stable methane gas sensors, RSC Adv. 8 (2018) 24268–24275, https://doi.org/10.1039/c8ra03242d.

[26] H.S. Yoon, J.H. Kim, H.J. Kim, H.N. Lee, H.C. Lee, Preparation of gas sensors with nanostructured SnO2 thick films with different Pd doping concentrations by an ink dropping method, J. Korean Ceram. Soc. 54 (2017) 243–248, https://doi.org/10.4191/kcers.2017.54.3.10.

[27] G. Fedorenko, L. Oleksenko, N. Maksymovych, G. Skolyar, O. Ripko, Semiconductor gas sensors based on Pd/SnO2 nanomaterials for methane detection in air, Nanoscale Res. Lett. 12 (2017), https://doi.org/10.1186/s11671-017-2102-0.

[28] D.D. Spasov, N.A. Ivanova, A.S. Pushkarev, I.V. Pushkareva, N.N. Presnyakova, R.G. Chumakov, M.Y. Presnyakov, S.A. Grigoriev, V.N. Fateev, On the influence of composition and structure of carbon-supported Pt-SnO2 hetero-clusters onto their electrocatalytic activity and durability in PEMFC, Catalysts 9 (2019), https://doi.org/10.3390/catal9100803.

[29] D. Xue, P. Wang, Z. Zhang, Y. Wang, Enhanced methane sensing property of flower-like SnO2 doped by Pt nanoparticles: a combined experimental and first-principle study, Sensor. Actuator. B Chem. 296 (2019), https://doi.org/10.1016/j.snb.2019.126710.

[30] S. Keshtkar, A. Rashidi, M. Kooti, M. Askarieh, S. Pourhashem, E. Ghasemy, N. Izadi, A novel highly sensitive and selective H2S gas sensor at low temperatures based on SnO2 quantum dots-C60 nanohybrid: experimental and theory study, Talanta 188 (2018) 531–539, https://doi.org/10.1016/j.talanta.2018.05.099.

[31] M.A. Abdulsattar, A.L. Resne, S. Abdullah, R.J. Mohammed, N.K. Alared, E.H. Naser, Chlorine gas sensing of SnO 2 nanoclusters as A function of temperature: a DFT study, Surf. Rev. Lett. 26 (2019), https://doi.org/10.1142/S0218625X1850172X.

[32] M.A. Abdulsattar, S.S. Batros, A.J. Addie, Indium doped SnO 2 nanostructures preparation and properties supported by DFT study, Superlattice. Microst. 100 (2016) 342–349, https://doi.org/10.1016/j.spmi.2016.09.042.

[33] Y. Ren, Q. Wang, X. Zhou, Y. Gao, G. Zhao, Fabrication of textured rough SnO2:F films on glass using TiO2Film as a buffer layer, J. Electron. Mater. 46 (2017) 6864–6869, https://doi.org/10.1007/s11664-017-5733-0.

[34] M. Thirumoorthi, J.T.J. Prakash, Effect of F doping on physical properties of (211) oriented SnO2 thin films prepared by jet nebulizer spray pyrolysis technique, Superlattice. Microst. 89 (2016) 378–389, https://doi.org/10.1016/j.spmi.2015.11.023.

[35] Q. Kuang, X. Zhou, L.S. Zheng, Hexagonal ZnO/SnO2 core-shell micropyramids: epitaxial growth-based synthesis, chemical conversion, and cathodoluminescence, Inorg. Chem. Front. 1 (2014) 186–192, https://doi.org/10.1039/c3qi00064h.

[36] N. Somjaijaroen, R. Sakdanuphab, N. Chanlek, P. Chirawatkul, A. Sakulkalavek, Simultaneous O2 plasma and thermal treatment for improved surface conductivity of Cu-Doped SnO2 films, Vacuum 166 (2019) 212–217, https://doi.org/10.1016/j.vacuum.2019.05.017.

[37] V. Vasanthi, M. Kottaisamy, K. Anitha, V. Ramakrishnan, Yellow emitting Cd doped SnO2 nanophosphor for phosphor converted white LED applications, Mater. Sci. Semicond. Process. 85 (2018) 141–149, https://doi.org/10.1016/j.mssp.2018.06.001.

[38] Russell D. Johnson III, NIST Computational Chemistry Comparison and Benchmark Database NIST Standard Reference Database Number 101 Release 18, 2016.

[39] G.E.S.M.J. Frisch, G.W. Trucks, H.B. Schlegel, B.M.M.A. Robb, J.R. Cheeseman, G. Scalmani, V. Barone, H.P.H.G.A. Petersson, H. Nakatsuji, M. Caricato, X. Li, M.H.A.F. Izmaylov, J. Bloino, G. Zheng, J.L. Sonnenberg, T.N.M. Ehara, K. Toyota, R. Fukuda, J. Hasegawa, M. Ishida, J.Y. Honda, O. Kitao, H. Nakai, T. Vreven, J.A. Montgomery, E.B.J.E. Peralta, F. Ogliaro, M. Bearpark, J.J. Heyd, J.N.K.N. Kudin, V.N. Staroverov, R. Kobayashi, J.T.K. Raghavachari, A. Rendell, J.C. Burant, S.S. Iyengar, J.B.C.M. Cossi, N. Rega, J.M. Millam, M. Klene, J.E. Knox, R.E.S.V. Bakken, C. Adamo, J. Jaramillo, R. Gomperts, J.W.O.O. Yazyev, A.J. Austin, R. Cammi, C. Pomelli, G.A.V.R.L. Martin, K. Morokuma, V.G. Zakrzewski, A.D.D.P. Salvador, J.J. Dannenberg, S. Dapprich, J.C.O. Farkas, J.B. Foresman, J.V. Ortiz, D.J. Fox, Gaussian 09, 2009.

[40] J. Mittal, K.L. Lin, Sn/SnO hybrid graphene for thermal interface material and interconnections with Sn hybrid carbon nanotubes, Mater. Sci. Eng. B Solid-State Mater. Adv. Technol. 253 (2020), https://doi.org/10.1016/j.mseb.2019.114485.

[41] A. Omidvar, Indium-doped and positively charged ZnO nanoclusters: versatile materials for CO detection, Vacuum 147 (2018) 126–133, https://doi.org/10.1016/j.vacuum.2017.10.023.

[42] H. Ha, M. Yoo, H. An, K. Shin, T. Han, Y. Sohn, S. Kim, S.R. Lee, J.H. Han, H.Y. Kim, Design of reduction process of SnO2 by CH4 for efficient Sn recovery, Sci. Rep. 7 (2017), https://doi.org/10.1038/s41598-017-14826-7.

[43] N. Van Toan, N. Viet Chien, N. Van Duy, H. Si Hong, H. Nguyen, N. Duc Hoa, N. Van Hieu, Fabrication of highly sensitive and selective H2 gas sensor based on SnO2 thin film sensitized with microsized Pd islands, J. Hazard Mater. 301 (2016) 433–442, https://doi.org/10.1016/j.jhazmat.2015.09.013.

[44] M.A. Abdulsattar, S.A. Majeed, A.M. Saeed, Electronic, structural, and vibrational properties of α-sn nanocrystals built from diamondoid structures: ab initio study, IEEE Trans. Nanotechnol. 13 (2014) 1186–1193, https://doi.org/10.1109/TNANO.2014.2352281.